JOURNAL OF VIROLOGY, May 2007, p. 5339–5348 Vol. 81, No. 10
0022-538X/07/$08.00+0 doi:10.1128/JVI.02427-06

Importance of the Penultimate Positive Charge in Mouse Hepatitis Coronavirus A59 Membrane Protein▽

Sandhya Verma,[2]† Lisa A. Lopez,[1,2,3]† Valerie Bednar,[2] and Brenda G. Hogue[1,2]*

School of Life Sciences,[1] The Biodesign Institute, Center for Infectious Diseases and Vaccinology,[2] and Molecular and Cellular Biology Graduate Program,[3] Arizona State University, Tempe, Arizona 85287-5401

Received 4 November 2006/Accepted 15 February 2007

The coronavirus membrane (M) protein carboxy tail interacts with the nucleocapsid during virus assembly. Previous studies demonstrated that the two terminal residues are important, and the charged residue (R227) in the penultimate position in the mouse hepatitis coronavirus (MHV) A59 M protein was suggested to participate in intermolecular interactions with negative charges in the nucleocapsid (N) protein. To determine the significance of the positive charge at position 227, we substituted the arginine with lysine (K), aspartic acid (D), glutamic acid (E), or alanine (A) and studied these by reverse genetics in the context of a MHV full-length infectious clone. Viruses with wild-type phenotype were readily recovered with the K or A substitutions. In contrast, negative-charge substitutions were not tolerated as well. In all recovered R227D viruses the negative charge was replaced with heterologous residues resulting from apparent template switching during negative-strand synthesis of subgenomic RNA 7. An additional second-site compensatory V202I substitution was present in some viruses. Recovered R227E viruses had second-site changes within the M protein carboxy tail that were partially compensatory. Significantly, most of the second site changes in the R227E mutant viruses were previously shown to compensate for the removal of negative charges in the N protein. Our results strongly indicate that a positive charge is not absolutely required. It is clear that other regions within the tail must also be involved in helping mediate interactions between the M protein and the nucleocapsid.

Coronaviruses are enveloped positive-stranded RNA viruses that belong to the *Coronaviridae* family in the *Nidovirales* order. The viruses are medically important viruses that cause primarily respiratory and enteric infections in humans and a wide range of animals. Recently, new human coronaviruses, including the severe acute respiratory syndrome (SARS) coronavirus (SARS-CoV), HCoV-NL63, and HCoV-HKU1 were identified, which significantly increased the interest in understanding this family of viruses and development of therapeutic treatments against them (9, 16). Understanding key interactions during virus assembly can provide insight to potential targets for antiviral and vaccine development.

The coronavirus virion envelope contains at least three integral membrane proteins. The spike (S), membrane (M), and envelope (E) proteins are anchored in the virion envelope. The S glycoprotein is the receptor-binding protein that facilitates infection through fusion of viral and cellular membranes and is the major target of neutralizing antibodies (14). The M glycoprotein is a major component of the envelope that plays an important role in virus assembly (8, 17, 24, 26, 31). The E protein is a minor component of the viral envelope that plays an important, but not yet fully defined role(s) during the virus life cycle (1, 4, 31). The nucleocapsid (N) protein encapsidates the viral genome as a helical nucleocapsid inside the virion (5, 20). Assembly of these components into virions occurs at intracellular membranes in the region of the endoplasmic reticulum Golgi intermediate compartment (ERGIC) (18, 30).

The focus of this report is the M protein. It is the most abundant protein in the viral envelope. It plays a key role in virus assembly through interactions with itself, the other envelope proteins, and the nucleocapsid (7, 8, 11, 19, 24, 26). The overall structure of the M protein is conserved across the family. The type III protein consists of three hydrophobic transmembrane domains, a short amino terminus exposed on the outside of the virion, and a long carboxy tail that consist of an amphiphilic region followed by a hydrophilic domain (Fig. 1) (27). The protein localizes in the Golgi when expressed alone (17, 18). Coexpression of the M and E proteins in the absence of the other viral components is sufficient for assembly of virus-like particles (VLPs) (1, 4, 31).

In the present study, we examined the importance of the penultimate charged residue in the mouse hepatitis coronavirus (MHV) A59 M protein tail (Fig. 1). Previous studies demonstrated that the extreme carboxy residues are very important in virus assembly (6, 19). The presence of a conserved charged residue positioned close to the end of the hydrophilic domain prompted us to ask whether the specific charge is important (Fig. 1). The positively charged arginine (R) in MHV A59 M at position 227 was changed to lysine (K), alanine (A), aspartic acid (D), or glutamic acid (E) and studied by reverse genetics using a full-length MHV infectious genome. The results show that the presence of a positive charge is not absolutely required at this position. Replacement of the amino acid with either positively charged lysine or neutrally charged alanine was not disruptive since stable viruses were readily isolated that are phenotypically like the wild-type (WT) virus. However, placement of a negatively charged residue at this position is clearly not preferred.

* Corresponding author. Mailing address: Biodesign Institute, P.O. Box 875401, Arizona State University, Tempe, AZ 85287-5401. Phone: (480) 965-9478. Fax: (480) 727-7615. E-mail: Brenda.Hogue@asu.edu.
† S.V. and L.A.L. contributed equally to this study.
▽ Published ahead of print on 28 February 2007.

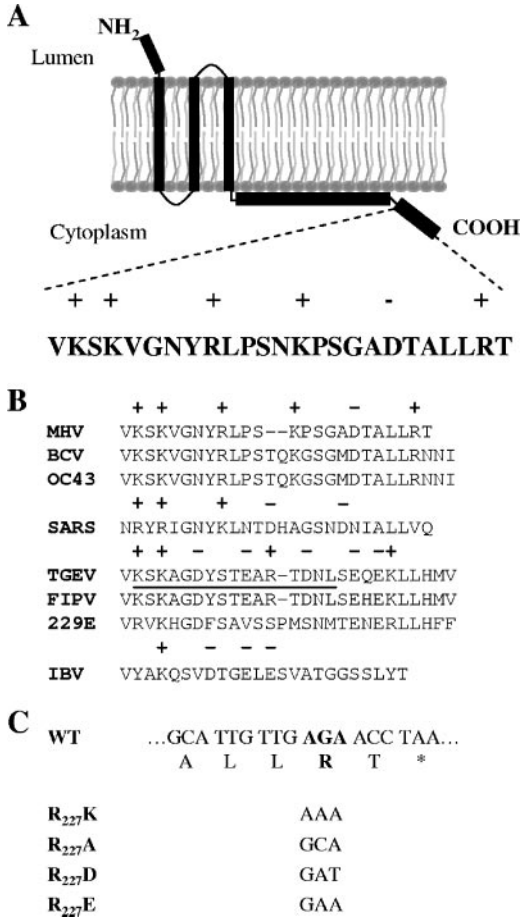

FIG. 1. M protein hydrophilic tail and amino acid substitutions at R227. (A) A schematic illustrating the topological structure of the MHV A59 M protein is shown (27). The lumen and cytoplasmic sides correspond to inner and outer sides of the ERGIC/Golgi membranes where MHV assembles. (B) An alignment of M protein carboxy hydrophilic tails from representatives of group II MHV, bovine coronavirus (BCV), human coronavirus OC43, SARS-CoV (SARS); group I TGEV, feline infectious peritonitis (FIPV), human coronavirus 229E; group III infectious bronchitis virus (IBV) was generated by CLUSTAL W (29). TGEV residues that were previously mapped to interact in vitro with the nucleocapsid are underlined (10). Positively and negatively charged amino acids are indicated above the sequences by plus and minus signs, respectively. (C) Amino acid substitutions and the corresponding codon changes introduced in place of R227 are indicated below the WT amino acid sequence of the hydrophilic domain.

MATERIALS AND METHODS

Cells and viruses. WT MHV A59 and infectious cloned viruses were grown in mouse 17 clone 1 (17Cl1) or L2 cells. Virus titers were determined in L2 cells. Cells were maintained in Dulbecco modified Eagle medium supplemented with 5 to 10% heat-inactivated fetal calf serum. Baby hamster kidney cells expressing the MHV Bgp 1a receptor (34) were maintained in Glasgow modified Eagle medium supplemented with 5% heat-inactivated fetal calf serum, 10% tryptose phosphate broth, and Geneticin (G418).

Construction of charge substitution mutants. Site-directed mutations were introduced into plasmid pGEM-5Zf(−)M-N, a pGEM5Zf(−) vector (Promega) containing the entire M and N genes (EcoRV-SacI fragment). A protocol based on the gene editor site-directed mutagenesis system from Promega was used with the primers shown in Table 1. All mutations were confirmed by sequencing the region between the NheI and BssHII unique restriction sites within the M and N genes, respectively, prior to being shuttled into MHV G clone in place of the WT fragment (34).

Generation of mutant viruses. Mutant viruses were generated by using an MHV A59 infectious clone (34). Full-length cDNA clones were assembled basically as previously described (32). Plasmids containing the cDNA cassettes spanning the MHV genome were digested with the appropriate restriction enzymes, gel purified, and ligated overnight to assemble the full-length genomic cDNA clone. Ligated cDNAs were extracted with phenol-chloroform and ethanol precipitated. RNA transcripts were made by using the mMessage mMachine T7 transcription (Ambion) reagents supplemented with additional GTP. The MHV nucleocapsid gene was transcribed from pMHV-A59 N (3) by using T7 RNA polymerase and polyadenylated using Ambion's poly(A) tailing system.

Full-length MHV infectious cloned genomic RNA and N transcripts were electroporated into BHK-MHVR cells (10^7 cells/ml) in OptiMEM (Invitrogen). RNA transcripts were electroporated in a 4-mm gap cuvette with three electrical pulses of 850 V at 25 μF by using a Bio-Rad Gene Pulser II electroporator. Transfected cells were monitored for fusion 12 to 48 h after electroporation.

An aliquot of the frozen stock from the electroporated cells was used to infect L2 cells. The media were harvested from the infected cells at approximately 24 h postinfection (p.i.). Total RNA was extracted from cells remaining adhered to the flasks using Ambion's RNAqueous-4PCR extraction buffers. Reverse transcription-PCR (RT-PCR) products from the RNA were sequenced directly to confirm the presence of the mutations in the M gene. Ten to twenty plaques were subsequently isolated from the electroporated cell-medium virus stock. Plaque-purified viruses were passaged onto L2 cells. RNA was extracted from the infected cells at approximately 24 h p.i. RT-PCR was performed, and the entireties of the E, M, and N genes were sequenced. Selected plaque purified viruses were amplified on L2 or Prc/1 cells through five passages, at which time the sequences of the E, M, and N genes, and in some cases the 3′ end of the S gene and the packaging signal region in gene 1b, were again confirmed.

Growth kinetics. Growth kinetic experiments were carried out in 17Cl1 cells infected with P5 virus stocks. Cell culture supernatants were collected at various times p.i. Titers were determined by plaque assay on L2 cells. At approximately 48 to 72 h p.i., the agarose-medium overlays were removed before cells were stained with crystal violet.

Analysis of VLPs. BHK-21 cells were seeded 1 day prior to achieving 70 to 80% confluence for infection at a multiplicity of infection (MOI) of 5 with vaccinia virus vTF7-3 that expresses T7 RNA polymerase (13). Cells were transfected with pcDNA3.1 plasmids containing either WT or mutated M genes singly and in combination with the WT E gene immediately after infection using Lipofectamine (Invitrogen Life Technologies). Cells were incubated in OptiMEM medium at 37°C for 12 h, at which time the medium and intracellular cytoplasmic lysates were harvested. Cells were lysed on ice in a buffer containing 100 mM Tris, 100 mM NaCl, 0.5% Triton X-100, and 1 mM phenylmethylsulfonyl fluoride. The media were clarified at 14,000 × *g* for 15 min at 4°C. VLPs were collected by pelleting the clarified medium through a 30% sucrose cushion by ultracentrifugation for 3 h at 4°C in a Beckman SW55Ti rotor at 30,000 rpm. Pellets were resuspended directly in Laemmli sodium dodecyl sulfate-polyacrylamide gel electrophoresis (SDS-PAGE) sample loading buffer. Intracellular and extracellular samples were analyzed by SDS-PAGE. Proteins were transferred to polyvinylidene difluoride membranes and analyzed with anti-MHV M A03 (kindly provided by Kathryn Holmes, University of Colorado Health Sciences) and an anti-MHV E antibody (L. A. Lopez and B. G. Hogue, unpublished data). After incubation with appropriate secondary antibodies, the blots were visualized by chemiluminescence (Pierce). Protein products were quantified by densitometric scanning of the fluorograms and analyzed by using ImageQuant software (Molecular Dynamics).

Indirect immunofluorescence. BHK cells were transfected with pCAGGS (25) plasmids containing the WT or mutant M genes to determine the localization of the proteins. Cells were plated on two-well glass slides 1 day before transfection with Lipofectamine. At 16 h after transfection, cells were washed with phosphate-buffered saline (PBS) and fixed in methanol for 15 min at −20°C. After one additional wash with PBS, the cells were blocked with 0.2% gelatin in PBS for 2 h. Slides were then incubated with a mixture of anti-MHV M J1.3 and J2.7 monoclonal antibodies (12) and rabbit anti-giantin antibodies for 2 h at room temperature. Cells were washed with 0.2% gelatin in PBS before incubation with fluorescein isothiocyanate-labeled anti-mouse and AlexaFluor labeled anti-rabbit secondary antibodies. Cells were washed extensively with PBS containing 0.2% gelatin and a final wash with PBS alone before being mounted in ProLong Gold antifade reagent (Molecular Probes) plus DAPI (4′,6′-diamidino-2-phenylindole) to stain nuclei. Images were viewed by using an epifluorescence Nikon inverted microscope (Nikon, Inc., Melville, NY) with MetaMorph imaging soft-

TABLE 1. Primers used in this study

Primer	Sequence	Genomic location	Polarity	Purpose
R227A	TTTAGATTAGGT**TGC**CAACAATGCGGTGTCCGC	29631–29663	Reverse	R227→A mutation
R227K	TTTAGATTAGGT**TTT**CAACAATGCGGTGTCCGC	29631–29663	Reverse	R227→K mutation
R227D	TTTAGATTAGGTA**TC**CAACAATGCGGTGTCCGC	29631–29663	Reverse	R227→D mutation
R227E	TTTAGATTAGGT**TTC**CAACAATGCGGTGTCCGC	29631–29663	Reverse	R227→E mutation
MHV M-N(+)	CCACCTCTACATGCAAGGTGTTAAGC	29429–29454	Forward	RT-PCR
MHV M-N(−)	GGTCTGCCACAACCTTCTCTATCTG	31132–31156	Reverse	RT-PCR
MHV E-M(+)	CAGAACTGTCCAACAGGCCGTTAGCAAG	28626–28653	Forward	RT-PCR
MHV E-M(−)	GCAACCCAGAAGACACCTTCAATGC	30102–30126	Reverse	RT-PCR
PackSignPCRFor	TATTGACGTGTGCTGGAGTCAC	19951–19972	Forward	RT-PCR
PackSignPCRRev	CATAACCAGGTTTCCAGTCAGC	20852–20873	Reverse	RT-PCR
Leader	TATAAGAGTGATTGGCGTCCGTACGT	1–26	Forward	RT-PCR
MHV M reverse	CGGTACCTTTCATATCTATAC	29350–29370	Reverse	Sequencing
MHV G 4 reverse	AGTCTGCTTTGGCTGATTCCTTC	29805–29827	Reverse	Sequencing
MHV 6 reverse	TTCCTGAGCCTGTCTACG	30860–30877	Reverse	Sequencing
MHV 7 forward	ATTCTGGTGGTGCTGATGAACC	30678–30699	Forward	Sequencing
MHV G8 forward	GGCAGAAGCTCCTCTGTAAACC	29705–29726	Forward	Sequencing
E reverse	CTCGTCGGCCGTCCATTGATAGAC	29001–29024	Reverse	Sequencing
PackSignSeqFor	TTAAGAAGTGCCGGAATGG	20106–20124	Forward	Sequencing
PackSignSeqRev	TGCTAGAGTCGTATGTCAC	20612–20630	Reverse	Sequencing

[a] Codon changes are indicated in boldface.

ware (Universal Imaging Corp., Downingtown, PA). Images were processed by using Adobe Photoshop.

RESULTS

Construction of charge substitution mutants at R227. To examine the importance of the positive charge at the penultimate position in the carboxy tail of the MHV M protein, R227 was changed to positively charged lysine (K), neutrally charged alanine (A), or the negatively charged residues aspartic acid (D) or glutamic acid (E) (Fig. 1). The effects of the mutations were analyzed for the ability of the mutant proteins to participate in virus-like particle (VLP) assembly and by reverse genetics in the context of genetically engineered viruses using a full-length MHV A59 infectious clone.

Effect of charge substitutions on M localization. Initially, the charge substitution mutants were expressed in BHK cells in parallel with the WT M protein to determine whether any of the changes affected normal cellular localization of the proteins. It is very well established that MHV M localizes to the Golgi (17). The WT and mutant proteins were expressed under the control of the chicken β-actin promoter using the pGAGGS vector and examined by immunofluorescence (25). Each mutant localized like the WT M protein in the Golgi (Fig. 2). Localization was confirmed by colocalization with the Golgi marker giantin. This indicated that the charge substitutions do not affect the normal transport and localization of the protein. Each of the mutant proteins also exhibited the same profile that is characteristic of the O-linked glycosylated WT protein when they were examined by SDS-PAGE and Western blotting (Fig. 3).

Effect of charge substitutions on VLP assembly. To determine whether the M mutants were competent to participate in assembly and release of VLPs, each mutant protein was coexpressed with the WT E protein. The proteins were expressed under the control of the T7 promoter using the vaccinia virus recombinant vTF7-3 that expresses T7 RNA polymerase (13). At 12 h p.i. the media were removed from cells and the cell

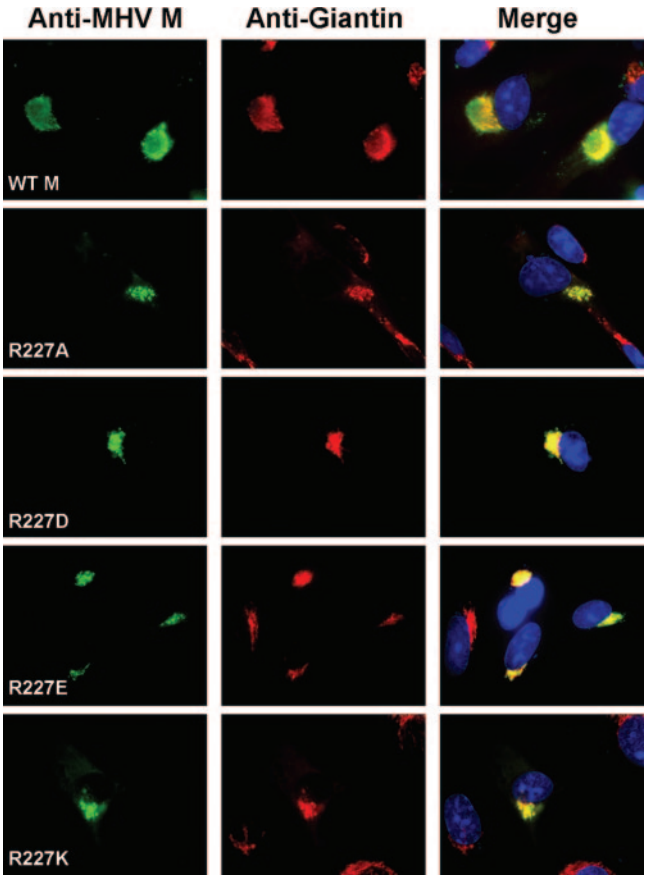

FIG. 2. Localization of WT M and mutant proteins. BHK-21 cells were transfected with the pCAGGS vector containing WT, R227A, R227D, R227E, or R227K M genes. Cells were fixed and analyzed by immunofluorescence with mouse antibodies against M. Colocalization of the proteins with the resident Golgi protein giantin is represented in the merged images by yellow. Nuclei were stained with DAPI. Fluorescein isothiocyanate-conjugated mouse and AlexaFluor 594-conjugated rabbit secondary antibodies were used to visualize the localization of the M and giantin proteins, respectively.

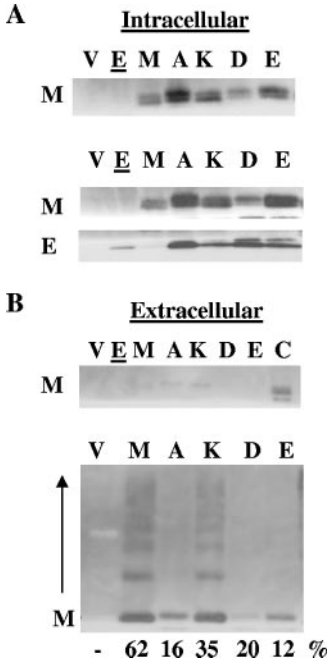

FIG. 3. Effect of R_{227} substitutions on VLP production. VLPs were produced in BHK-21 cells using vaccinia virus recombinant vTF7.3 that expresses T7 RNA polymerase (13). After infection, the cells were transfected with plasmids containing the WT, R227A, R227K, R227E, or R227D M genes singly (A and B, upper panels) or in combination with the WT E gene (underlined) (A and B, lower panels) under the control of a T7 promoter. The WT M and mutant proteins are designated M and the single-letter amino acid substitutions for each mutant, respectively. Proteins from control cells transfected with empty vector (V) were analyzed in lane 1 of each panel. The M protein was run as a marker (lane C) in parallel with samples from the extracellular fraction from cells expressing the protein alone (B, upper panel). Intracellular cell lysates (A) and pelleted extracellular VLPs (B) were analyzed by Western blotting. Half of the pelleted VLP fractions and 8% of the total intracellular fractions were analyzed by SDS-PAGE. Protein products were quantified by densitometric scanning and analyzed by using ImageQuant software. VLP release was calculated as the percentage of the extracellular M protein to the total M (intracellular plus extracellular) protein for each gene. The arrow in the lower panel highlights the multiple forms of the M protein that are sometimes observed when the protein is analyzed by SDS-PAGE.

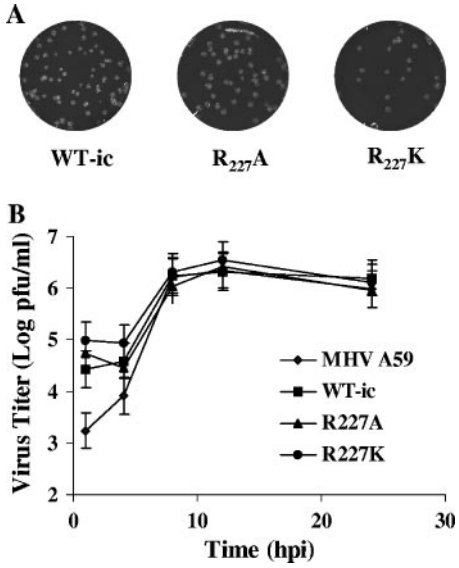

FIG. 4. Growth kinetics and plaque morphologies of the WT, R227K, and R227A viruses. (A) The plaque sizes and morphologies of WT and the R227K- and R227A-substitution viruses were analyzed in mouse L2 cells. (B) Mouse 17Cl1 cells were infected with WT and mutant viruses at an MOI of 10. Plaque titrations from the indicated time points were performed in mouse L2 cells.

monolayers were lysed. VLPs were isolated from clarified media by centrifugation through a sucrose cushion. Cytoplasmic lysates and the extracellular pelleted material were analyzed by SDS-PAGE and Western blotting (Fig. 3). All of the mutants were capable of forming VLPs, as indicated by the presence of extracellular M. The amount of extracellular M, which is used as the indicator for VLPs (1, 4, 31), was compared to the total amount of intracellular plus extracellular M. The K substitution appeared to have the least effect on the ability of the protein to participate in VLP assembly, which suggests that the M protein with a positive charge at position 227 may be functionally more competent to participate in assembly of VLPs.

The positive charge at position 227 is not absolutely required for virus production. To examine the direct effect of the amino acid substitutions on virion assembly in the context of the virus, R227 codon mutations were introduced into an MHV infectious clone (34). After electroporation, viruses were readily recovered for both R227K and R227A mutants. Both mutant viruses appeared to be phenotypically like the WT virus. Multiple plaques were isolated from the mutant viruses and the WT control virus. Total RNA was extracted from cells infected with passage 2 (P2) of the plaque-purified viruses and used as the template for RT-PCR of the genome encompassing the M, E, and N genes. Direct sequencing of amplified products showed that the introduced codon changes were present in each of the mutant viruses and that no additional changes were present in the remainder of the M gene or in the E and N genes.

Multiple plaque-purified viruses were subsequently passaged three additional times in 17Cl1 cells. Direct sequencing of RT-PCR products amplified from the 3′ end of total viral RNA from cells infected with P5 viruses confirmed that the codon changes at position 227 were present. No additional changes in the remainder of the M gene or in the N or E genes had arisen during passage of the viruses. This indicates that the mutations were stably maintained. Both mutants exhibited growth properties and plaque phenotypes essentially identical to parental infectious cloned MHV and WT MHV stock virus (Fig. 4). The results indicate that a positive charge is not absolutely required at amino acid position 227.

A negative charge substitution in place of R227 has a significant impact on virus growth. In contrast to the R227K and R227A mutant viruses that were phenotypically like the WT virus, the substitution of negatively charged D and E residues at position 227 had a drastically opposite effect. Only a few small fusion foci were observed after electroporation of the mutants, and no fusion was observed when the media off these cells were transferred onto 17Cl1 cells.

After we confirmed the replication competency of the mutants, L2 cells were infected with supernatant off the electro-

TABLE 2. Summary of known second-site changes recovered from mutant viruses with changes in M R227 and N DD440-441

Mutant viruses	Passage	No. of plaques analyzed	R_{227} mutation retained	Change(s) in M[a]	Change(s) in N
Membrane protein					
R_{227}D #1	P5	20	No	$D_{227}T_{228}$→NLI	
		2	No	$D_{227}T_{228}$→NLI, **V_{202}→I**	
R_{227}D #2	P2	10	No	$D_{227}T_{228}$→NLI	
R_{227}E	P5				
23		1	Yes	None	
29		1	Yes	**I_{128}T**	
64		1	Yes	L_{155}F	
32, 43, 66, 68, 71		5	Yes	**Y_{156}H**	
MΔ2[b]				T_{185}I, D_{195}G, D_{195}N, G_{196}S, S_{206}F	Q_{437}L Q_{437}MMA
Nucleocapsid protein					
D_{440}R[c]					R_{425}G T_{428}N
D_{441}R[c]					R_{425}G A_{436}D
$DD_{440\text{-}441}$AA[c]					$SR_{424\text{-}425}$GG
$DD_{440\text{-}441}$AA[d]				**I_{128}T**, Y_{143}H, **Y_{156}H**, **V_{202}I**	Q_{437}L

[a] Second-site changes in boldface denote changes recovered independently from viruses with mutations in N or M.
[b] Kuo and Masters (19).
[c] Verma et al. (32).
[d] Hurst et al. (15).

porated BHKR cells since small centers of fusion are generally more easily observed in these cells. A few small fusion foci were observed, but only a small portion of the cells were fused even after 72 h p.i. Direct sequencing of RT-PCR products of M subgenomic RNA confirmed that the nucleotide substitutions in codon 227 were present in P1 of the mutant viruses. Neither mutant exhibited a temperature-sensitive phenotype since no growth advantage was observed when the viruses were grown at 33 or 39°C (data not shown).

Since the titers of the recovered R227D and R227E viruses were very low, both were blindly passaged in L2 cells to determine whether revertant or compensatory changes might arise to give the mutant viruses a growth advantage. By P5 the R227D virus exhibited a larger plaque phenotype and titers closer to that of the WT virus. On the other hand, the P5 R227E stock had a titer that was several logs lower and continued to give rise to small plaques.

Recovery of R227D viruses. Individual viruses were isolated from P5 of the R227D virus stock. The plaque-purified viruses were grown on L2 cells, and the M, E, and N gene regions were amplified by RT-PCR. Direct sequencing of the products from 22 R227D viruses revealed one major change (Table 2). Ten nucleotides were replaced by 13 heterologous nucleotides, which resulted in the R227D mutation and the terminal WT threonine being replaced by three heterologous amino acids: asparagine, leucine, and isoleucine (NLI) (Fig. 5). Two of the plaque-purified viruses (D54 and D55) contained an additional change where V_{202} was changed to an isoleucine (Table 2). Examination of the codons for the NLI residues that arose and dominated the population of viruses indicated that the changes most likely resulted from template switching during negative-strand synthesis of subgenomic RNA 7, the N mRNA (Fig. 5). A strand switch apparently occurred after the normal polymerase switch to copy the leader sequence back to the M gene coding region of the genome, resulting in the TAA residues within the transcription regulatory sequence (TRS) becoming the new stop codon for the M gene (Fig. 5B).

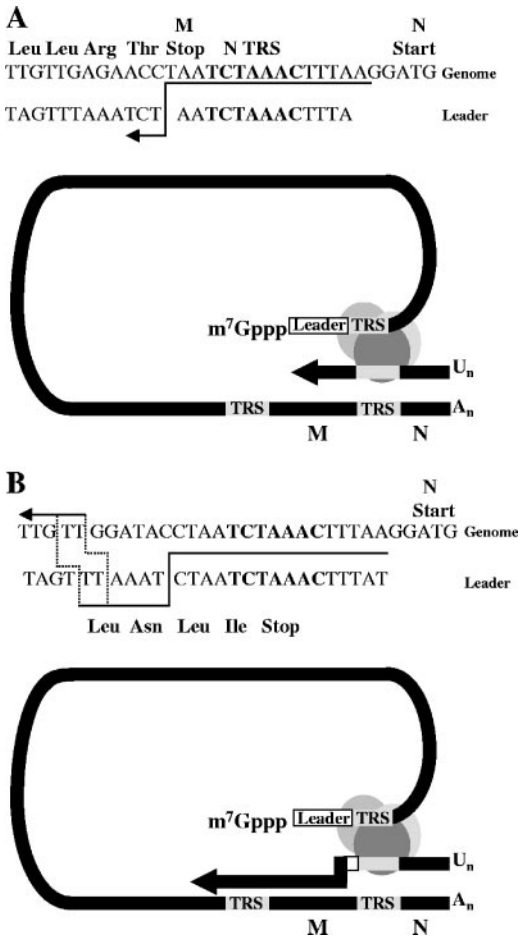

FIG. 5. Model for recovery of viruses with R227D mutations. A schematic adapted from the three-step model for coronavirus subgenomic RNA transcription (28, 35) is shown for mRNA 7 (N gene) transcription and addition of the leader (A) and the template switches resulting in removal of the R227D substitution (B) during discontinuous negative-strand synthesis.

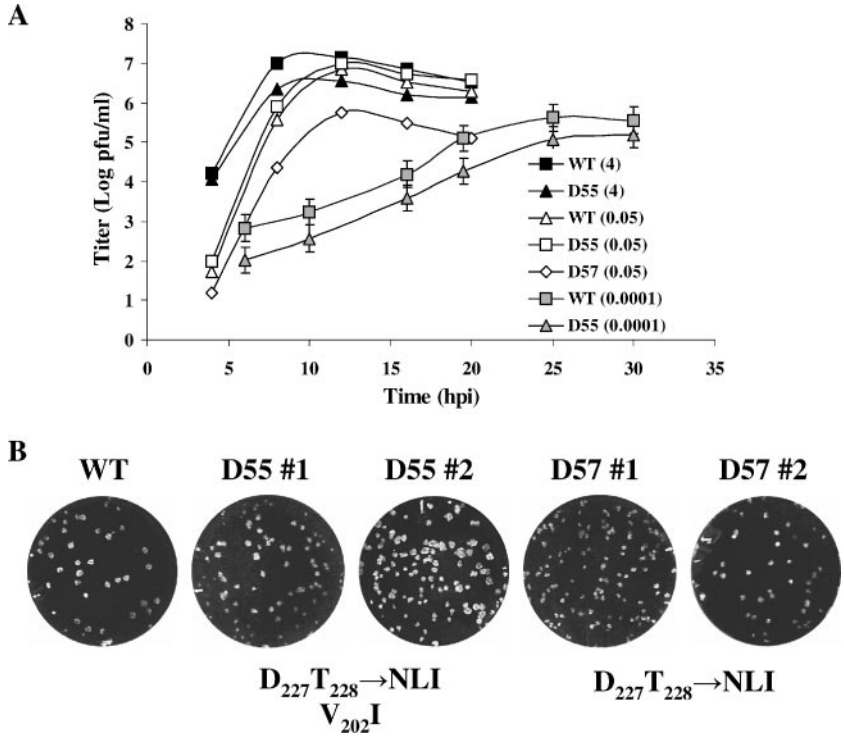

FIG. 6. Growth kinetics and plaque morphologies of recovered R227D viruses. (A) Mouse L2 cells were infected with WT and recovered plaque-purified viruses at the MOIs indicated for each virus. Error bars represent the relative deviation from the average for three independent experiments. (B) Plaque sizes and morphologies were analyzed in parallel with WT virus in mouse L2 cells. The numbers designate the originally recovered (#1) and reconstructed (#2) D55 and D57 viruses.

After we determined that the R227D P5 virus population was apparently dominated by a virus resulting from strand switching during negative-strand synthesis, a second independent virus clone was assembled that contained the R227D mutation. The recovered virus was passaged two times on L2 cells. Ten plaque-purified viruses were selected from P2 for growth on L2 cells. RT-PCR products from cells infected with the viruses were sequenced to analyze the M, E, and N genes. Interestingly, all of the viruses had undergone the same major change that was observed with the first R227D virus, where the last two residues were replaced by the NLI residues (Table 2). Retrospective examination of 13 plaque-purified viruses from P0 and P1 of the second virus clone showed that the R227D substitution was present in all but one of the viruses (data not shown). Twelve of the viruses had two additional changes in which isoleucine 128 and arginine 137 were changed to methionine and glycine, respectively. One virus contained the NLI replacement and no other changes. Analysis of 10 viruses from P2 showed that the latter dominated the population. This strongly suggested that removal of the negative charge must provide a growth advantage for the virus.

Three plaque-purified viruses (D55, D57, and D5) recovered from the R227D mutant viruses were analyzed for their growth properties. D55 and D57 were plaque purified from the first construction of the R227D virus. Both viruses contained the NLI replacement of the D227 substitution and the carboxy-terminal T228 residue. D55 also contained the valine-to-isoleucine change at position 202. The D5 virus was plaque purified from P1 of the second independent construction of the virus that was described above. The virus retained the R227D substitution but also had acquired the I128M and R137G changes. Initial analysis of the D5 virus revealed that the virus was very crippled, with a titer of approximately 10^2 PFU/ml and a very tiny plaque phenotype. Since the additional changes that arose after electroporation provided no growth advantage for the virus, the virus was not analyzed further. This apparently accounts for the observation that the virus was outcompeted by viruses with the D57 genotype.

D55 and D57 viruses were further examined after six passages: five on L2 cells and a final passage on 17Cl1 cells. Sequences from the M, N, and E genes showed no change other than those already observed in the initial analysis of the viruses. The P5 D55 virus grew to a titer $\sim 10^6$ PFU/ml, whereas the D57 virus stocks were 1 to 1.5 logs lower. The D55 virus exhibited a plaque morphology and size similar to the WT virus, whereas the D57 virus had a smaller plaque phenotype (Fig. 6). Both viruses were examined for their growth kinetics. Initially, L2 cells were infected with D55 and WT MHV at an MOI of 4. The D55 virus grew similar to the WT virus, yielding a slightly lower titer (Fig. 6). The growth of D57 was also examined, but cells were infected with an MOI of only 0.05 since the titer of the virus stock was lower than that of either the WT or D55 viruses. The D57 virus grew somewhat slower than either the WT or D55 viruses, reaching a peak titer at least a log lower at 12 h p.i. (Fig. 6). D55 was further compared to WT virus at a very low MOI of 0.0001, which further confirmed that the virus grew similarly (Fig. 6, gray symbols).

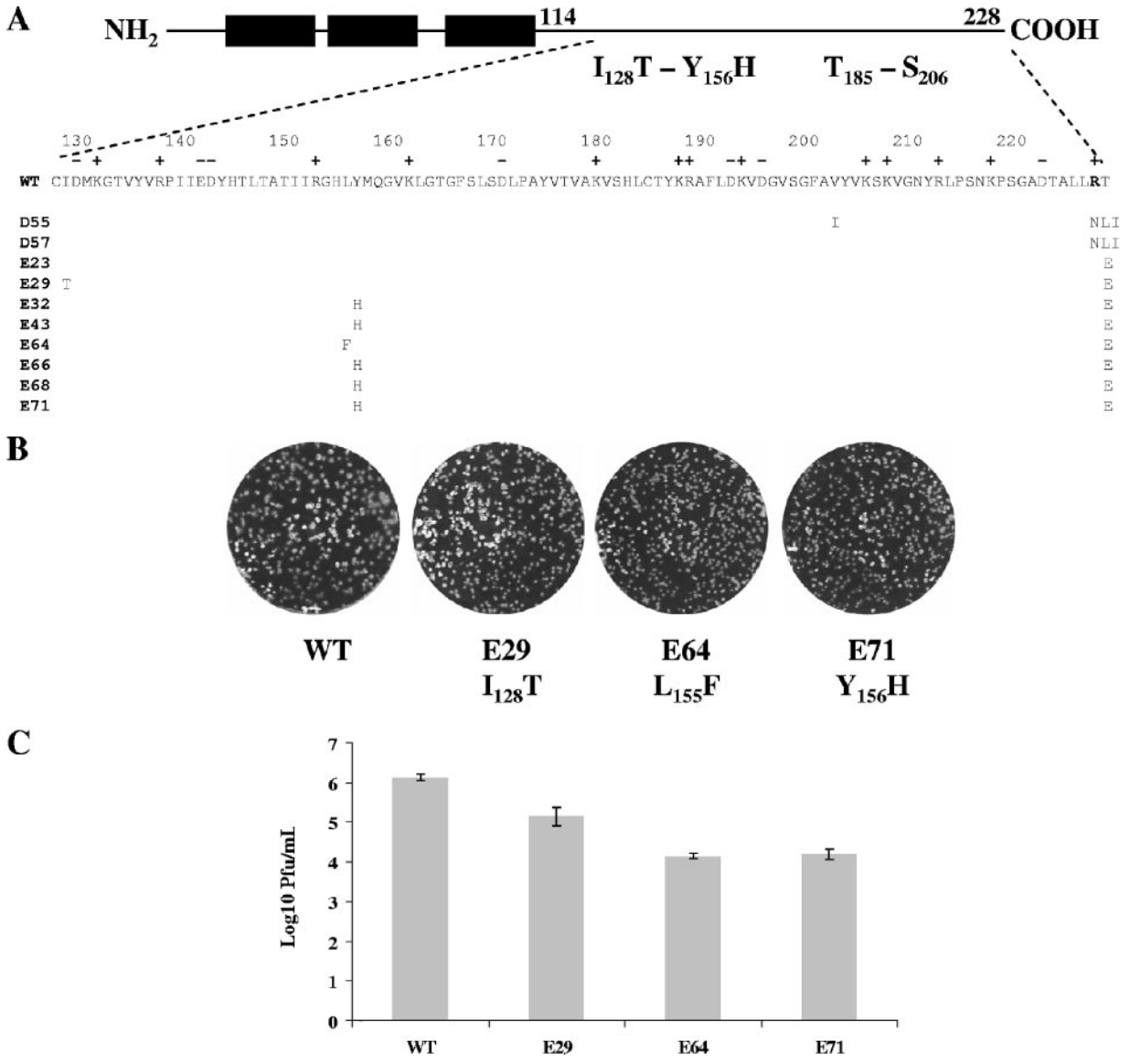

FIG. 7. Summary of recovered viruses with the R227E substitution. (A) Sequence analysis of the M gene from multiple recovered viruses with the R227E substitution is shown. The second-site amino acid changes are shown under the WT sequence. The D and E designations refer to the R227D and R227E viruses, and numbers refer to isolated plaques. (B) Plaque phenotypes were determined in mouse L2 cells in comparison with the WT virus for recovered R227E viruses. (C) Mouse L2 cells were infected with the WT or recovered viruses (E64, E71, or E29) at an MOI of 0.0001, and virus titers (intracellular plus extracellular) were measured by plaque assay in mouse L2 cells at 20 h p.i. The error bars represents the standard deviations of three independent measurements.

To confirm that the changes in the recovered D55 and D57 viruses were indeed responsible for the apparent growth advantage of the viruses, independent viruses were constructed that contained the NLI replacement of the terminal two residues or the V202I/NLI changes. The viruses that were recovered from the newly constructed clones exhibited growth and plaque size and/or morphology like those of the originally recovered D55 and D57 viruses, thus confirming that the changes were responsible for the growth advantage (Fig. 6B). Altogether, the results indicate that removal of the introduced negative charge at position 227 coupled with the $V_{202}I$ change provides a significant growth advantage compared to the R227D mutant without compensating changes. The two carboxy-terminal residues can be replaced by at least three heterologous residues, none of which are charged amino acids. This is consistent with the results from the R227A substitution. It also appears that template switching during negative-strand synthesis can be a driving force for selection of more fit viruses, at least those with mutations at the extreme carboxy end of the M gene.

Recovery of R227E viruses. An equivalent number of plaque-purified viruses were also isolated from P5 of the R227E mutant. However, unlike the R227D virus, many of the R227E viruses were extremely difficult to rescue. Isolated viruses gave rise to only a few fusion foci when placed on new cells and, even when centers of fusion were seen, the viruses

often failed to grow to significantly measurable titers when passaged a second time. Ultimately, only eight viruses were isolated that could be maintained through five passages (Fig. 7 and Table 2). These viruses were analyzed to identify any second-site changes. After P1 on L2 cells all eight viruses contained the glutamic acid substitution at position 227. However, five of the eight viruses (E32, E43, E66, E68, and E71) also had a new amino acid change at position 156 where the tyrosine was replaced by a histidine residue (Fig. 7 and Table 2). All of the viruses with the Y156H change were stable through P5. The other three viruses (E23, E29, and E64) contained only the glutamic acid substitution at position 227 through P2. However, by P5 two of these, while maintaining the R227E mutation, had undergone additional changes. Isoleucine (I) at position 128 was changed to threonine (T) in E29 and leucine (L) at position 155 was changed to phenylalanine (F) in E64 (Table 2). E29, E64, and E71 were passaged six times. No additional changes were present in the M, N, and E genes, the 3′ end of the S gene, or the packaging signal region.

Since the titers of the recovered viruses were very low, limited analysis of their growth properties could be done (Fig. 7). The E23 virus that contained only the R227E substitution had a much smaller plaque phenotype than WT virus and very low titer (data not shown). The E29 virus plaques were similar to WT, whereas E64 and E71 viruses yielded plaques that were somewhat smaller. All three viruses grew to titers that were at least 1.5 to 2.0 logs lower than WT virus (Fig. 7).

These results, combined with those from the R227D mutant, strongly argue that placement of a negatively charged amino acid at position 227 has a deleterious effect on the virus. Placement of a negative charge at this position is not absolutely lethal, but results in very crippled viruses. The changes that arose in the R227E appear to provide a slight growth advantage, but the growth properties of the viruses indicate that the changes are not sufficient to fully compensate for the introduced negative charge at position 227.

DISCUSSION

We examined the importance of the positive charge at the penultimate position in the carboxy tail of the MHV A59 M protein. Our results show that R227 can be replaced by another positive charge or by neutrally charged alanine since recovered viruses with these substitutions exhibited no other changes and growth properties like the WT virus. In contrast, the inability to isolate a mutant that retained the R227D substitution and the difficulty experienced with isolation of R227E viruses demonstrated that negatively charged residues at this position significantly cripple the virus. We conclude that while the positive charge is not absolutely required, a negative charge at this position is detrimental or at least is significantly crippling for the virus. Our results provide important new insight since this is the first examination of the relevance of the charge at position 227.

Earlier studies contributed significantly to our understanding of the importance of R227 for virus assembly. The importance of the two carboxy-terminal residues in the MHV M protein was first recognized when VLP and virus assembly were both found to be sensitive to changes in the extreme end of the tail of the protein (6). Deletion of the terminal residues, R227 and T228, or replacement of R227 with an A residue abrogated VLP formation. We were able to isolate VLPs with the R227A substitution. The levels of protein expression or sensitivity of detection could possibly account for this.

The initial attempt to isolate by recombination a virus lacking R227 and T228 suggested that the deletion was lethal; however, isolation of the MΔ2 virus lacking these residues was subsequently successful when a more stringent host range selection approach was used (6, 19). The MΔ2 virus that was isolated by Kuo and Masters had an extremely defective phenotype, exhibiting very small plaques and titers of $<10^4$ PFU/ml (19). After several passages, MΔ2 viruses were recovered that had second-site changes in the M or N proteins, some of which were shown to compensate for deletion of the terminal two amino acids (summarized in Table 2). The changes mapped within a region bounded by T185 and S206 in the M protein or in the region of Q437 in the N protein (19). The study provided the first genetic evidence for an interaction between the carboxy termini of MHV M and N proteins.

Two recent studies showed that negatively charged amino acids in the carboxy terminus of the MHV A59 N protein are important for virus assembly. Our lab and also that of Masters et al. independently identified a pair of aspartic acids (DD440-441) in the N protein that are key residues involved in virus assembly (15, 32). We recovered viruses with second-site changes in the N protein when either of the aspartic acids were replaced with positively charged arginine or when both were changed to alanine. We showed that the second-site changes were able to compensate for the amino acid substitutions (32) (Table 2). Our colleagues recovered a different set of compensatory changes that mapped to the N gene but, interestingly, they also recovered viruses with compensatory changes within the M gene (15). Four single residue changes in the M protein—I128T, Y143H, Y156H, and V202I—were recovered and subsequently shown to compensate for alanine substitutions at DD440-441 in the N protein (Table 2). Very significant to our study reported here, with the exception of the Y143H changes, all of the second-site changes identified by Hurst et al. in the M protein that compensated for their removal of negative charges in the N protein are ones that we independently identified when we replaced R227 in the M protein with a negative charge (R227D and R227E) (Table 2). When obviously key charged residues, DD440-441 in the N protein (15) or R227 in the M protein (the present study), are modified and these independently give rise to overlapping second-site suppressor or adaptive changes in the I128-Y156 region, this strongly argues that the domain is an important contributor to N-M interactions.

It was previously suggested that residues within the region between I_{128} and S_{206} in the M protein may influence the presentation of R227 for interaction with the N protein and also that a major determinant of M-N protein interaction could be a salt bridge between the M protein R227 and N protein D440-441 (19) (15). Our data strongly support the idea that other residues beyond R227 likely influence the way R227 is made accessible for interaction with the N protein. Our results suggest that intragenic changes further toward the amino end of the I128-Y156 region in the M protein are partially compensating changes in the context of a negative charge at position 227, even though the changes are fully compensating when

the negative charges at DD440-441 in the N protein are replaced by neutrally charged alanine (15). More importantly, our study tested the hypothesis that a salt bridge plays a role in mediating interaction between M R227 and N DD440-441. Our results strongly indicate that a negative charge is not preferred at position 227, which is consistent with the idea that opposite charge interactions in the M and N proteins are important. However, it is also clear that interactions between the two proteins can be provided through other types of interactions or interactions with other residues, since the charge was lost in our recovered R227D viruses. The carboxy-terminal half of the M protein, consisting of ~100 amino acids, is primarily amphiphilic except for the terminal ~25 hydrophilic residues. Based on our results and those from earlier studies (15, 19), it appears that two regions, I128-Y156 and T185-S206, within the amphiphilic domain are important and linked, at least functionally, in some way to the extreme end of the hydrophilic domain. It appears that there may be few possibilities for suppressing mutations at R227 since all of the recovered viruses thus far map within these relatively narrow 21- to 28-amino-acid regions and very few second-site changes were recovered.

Identification of residues some distance from R227 that apparently contribute to its functional role indicates that interactions between M and N must be driven by more than just the positive charge at this position and the negative charges at DD440-441. Further support for this was illustrated when we attempted to construct a double mutant virus with reciprocal charge changes: R227D in the M proteins paired with our previously described D440R, D441R, or DD440-441RR mutations in the N protein (32). Fusion foci were present after electroporation, a finding indicative of replication-competent genomic RNA, but multiple attempts to recover viable viruses were not successful. Hurst et al. also indicated that they were not able to merely switch the charges between R227 in the M protein and DD440-441 in the N protein (15). These researchers did note as well in their overall discussion that to their surprise a virus was constructed with R227 in the M protein replaced with two aspartic acid residues. No information was given about the growth properties of the virus or if second-site changes were present. Based on our experience with our negative-charge substitution mutants, we speculate that such a virus would exhibit a crippled phenotype like our R227E virus. Studies with transmissible gastroenteritis coronavirus (TGEV) M also argue that interaction with the nucleocapsid is based on more than a single charged residue. A region consisting of residues 233 to 257 (underlined in Fig. 1) in the TGEV M protein mediates interaction in vitro with viral nucleocapsids (11).

The apparent inability to isolate a mutant with the R227D substitution appears to have been driven by two template switches during negative-strand synthesis of subgenomic RNA 7, the N gene. This mechanism was also observed with the MΔ2 mutant (19). Several revertant viruses of the MΔ2 mutant that had the last two carboxy-terminal residues (R227 T228) deleted also apparently arose, as was suggested, by nonhomologous recombination between genomic and subgenomic RNAs. It was suggested that the revertants arose during negative-strand discontinuous transcription as a result of transcription collapse. Since then, a model was developed to describe how coronavirus subgenomic RNAs are likely produced during discontinuous transcription (35). The model proposes that the 5′ and 3′ ends of genomic RNA interact while serving as the template for negative-strand subgenomic RNAs (Fig. 5A). During transcription the template switch site, from the genome TRS region to the leader, are thought to be determined by the strength of the base pairing between the nascent negative-strand TRS complement and the leader TRS. Our results with the D55 and D57 viruses are consistent with the model. Based on this it is clear that two template switches, N gene TRS to leader and back to the genome, could account for how our recovered viruses with the NLI replacement of the $R_{227}D$ mutation likely arose (Fig. 5B). The residues are similar to the terminal residues in the M tail of BCoV and HCoV OC43 (Fig. 1); however, positively charge R precedes the NNI residues in these viruses. Why this mechanism so readily gave rise to recoverable viruses in the case of the R227D mutant but was never observed for our R227E mutant is perplexing. Preliminary analysis of the base pairing between the expected nascent negative-strand RNA and the TRS-L does not appear to explain the difference. Future studies will be necessary to determine why the two behave differently.

Understanding the role of the M carboxy tail in virus assembly is complicated by the multiple interactions that apparently occur between M and the other viral components. The protein interacts with itself (6, 8, 17) and also with the S protein (24, 26), in addition to interactions with the nucleocapsid (21–23). The transmembrane domains are particularly important for M-M interactions (8). Recently, the requirements for incorporation of S into MHV virions was mapped to the transmembrane domain and cytoplasmic tail of the protein (2, 33), but the requirements within the M protein are still not known. The M protein requirements for interaction with S have been studied only by coimmunoprecipitations (7). Deletion of the amphipathic domain in the M protein had a severe affect on M-S interaction, whereas deletion of the amino and extreme carboxy domains did not. Recent studies demonstrated that MHV M protein also interacts with the viral packaging signal and that this apparent interaction was sufficient for incorporation of a packaging signal-containing RNA into VLPs without expression of the N protein (21).

It is well established that charged residues play important functional roles in proteins. They may contribute to the overall structure by assisting in proper folding through interaction with oppositely charged amino acids. Basic residues may form electrostatic interactions with acidic phospholipids in cell membranes, which may be particularly relevant for the M protein tail that apparently is tightly associated with the membrane (27). The data presented here in combination with previous studies (15, 19) strongly support the importance of the penultimate charged R227 in the MHV A59 M protein, but the results clearly demonstrate that other residues within the tail must influence, whether directly or indirectly, interactions with N or possibly the negatively charged phosphate backbone of the RNA genome. Future studies will address the role of the region delineated by the second-site changes identified here and in the earlier study (15). Since the M protein is multifunctional, understanding the complexity of its interactions will require the development of assays to facilitate this effort and structural information for both the M tail and nucleocapsids.

ACKNOWLEDGMENTS

The study was supported by Public Health Service grant AI53704 from the National Institute of Allergy and Infectious Diseases to B.G.H. L.A.L. was supported in part by the American Society for Microbiology Robert D. Watkins Graduate Research Fellowship.

We are very grateful to Ralph Baric and Boyd Yount for providing us with the MHV reverse genetics system and helpful advice as we initially established the use of the infectious clone in our lab with this study. We thank Karen Malone for initial analysis of the MHV G clone and construction of the pGEM M-N plasmid, Yaralid Sotomayor for assistance with virus titrations, Angel Morrow for help with reconstruction of recovered D55 and D57 viruses, and all members of the Hogue lab for helpful discussions throughout the study.

REFERENCES

1. **Bos, E. C., W. Luytjes, H. V. van der Meulen, H. K. Koerten, and W. J. Spaan.** 1996. The production of recombinant infectious DI-particles of a murine coronavirus in the absence of helper virus. Virology **218:**52–60.
2. **Bosch, B. J., C. A. de Haan, S. L. Smits, and P. J. Rottier.** 2005. Spike protein assembly into the coronavirion: exploring the limits of its sequence requirements. Virology **334:**306–318.
3. **Cologna, R., J. F. Spagnolo, and B. G. Hogue.** 2000. Identification of nucleocapsid binding sites within coronavirus-defective genomes. Virology **277:** 235–249.
4. **Corse, E., and C. E. Machamer.** 2000. Infectious bronchitis virus E protein is targeted to the Golgi complex and directs release of virus-like particles. J. Virol. **74:**4319–4326.
5. **Davies, H. A., R. R. Dourmashkin, and M. R. Macnaughton.** 1981. Ribonucleoprotein of avian infectious bronchitis virus. J. Gen. Virol. **53:**67–74.
6. **de Haan, C. A., L. Kuo, P. S. Masters, H. Vennema, and P. J. Rottier.** 1998. Coronavirus particle assembly: primary structure requirements of the membrane protein. J. Virol. **72:**6838–6850.
7. **de Haan, C. A., M. Smeets, F. Vernooij, H. Vennema, and P. J. Rottier.** 1999. Mapping of the coronavirus membrane protein domains involved in interaction with the spike protein. J. Virol. **73:**7441–7452.
8. **de Haan, C. A., H. Vennema, and P. J. Rottier.** 2000. Assembly of the coronavirus envelope: homotypic interactions between the M proteins. J. Virol. **74:**4967–4978.
9. **Donnelly, C. A., A. C. Ghani, G. M. Leung, A. J. Hedley, C. Fraser, S. Riley, L. J. Abu-Raddad, L. M. Ho, T. Q. Thach, P. Chau, K. P. Chan, T. H. Lam, L. Y. Tse, T. Tsang, S. H. Liu, J. H. Kong, E. M. Lau, N. M. Ferguson, and R. M. Anderson.** 2003. Epidemiological determinants of spread of causal agent of severe acute respiratory syndrome in Hong Kong. Lancet **361:**1761–1766.
10. **Escors, D., J. Ortego, and L. Enjuanes.** 2001. The membrane M protein of the transmissible gastroenteritis coronavirus binds to the internal core through the carboxy terminus. Adv. Exp. Med. Biol. **494:**589–593.
11. **Escors, D., J. Ortego, H. Laude, and L. Enjuanes.** 2001. The membrane M protein carboxy terminus binds to transmissible gastroenteritis coronavirus core and contributes to core stability. J. Virol. **75:**1312–1324.
12. **Fleming, J. O., S. A. Stohlman, R. C. Harmon, M. M. Lai, J. A. Frelinger, and L. P. Weiner.** 1983. Antigenic relationships of murine coronaviruses: analysis using monoclonal antibodies to JHM (MHV-4) virus. Virology **131:** 296–307.
13. **Fuerst, T. R., E. G. Niles, F. W. Studier, and B. Moss.** 1986. Eukaryotic transient-expression system based on recombinant vaccinia virus that synthesizes bacteriophage T7 RNA polymerase. Proc. Natl. Acad. Sci. USA **83:**8122–8126.
14. **Gallagher, T. M., and M. J. Buchmeier.** 2001. Coronavirus spike proteins in viral entry and pathogenesis. Virology **279:**371–374.
15. **Hurst, K. R., L. Kuo, C. A. Koetzner, R. Ye, B. Hsue, and P. S. Masters.** 2005. A major determinant for membrane protein interaction localizes to the carboxy-terminal domain of the mouse coronavirus nucleocapsid protein. J. Virol. **79:**13285–13297.
16. **Kahn, J. S.** 2006. The widening scope of coronaviruses. Curr. Opin. Pediatr. **18:**42–47.
17. **Klumperman, J., J. K. Locker, A. Meijer, M. C. Horzinek, H. J. Geuze, and P. J. Rottier.** 1994. Coronavirus M proteins accumulate in the Golgi complex beyond the site of virion budding. J. Virol. **68:**6523–6534.
18. **Krijnse-Locker, J., M. Ericsson, P. J. Rottier, and G. Griffiths.** 1994. Characterization of the budding compartment of mouse hepatitis virus: evidence that transport from the RER to the Golgi complex requires only one vesicular transport step. J. Cell Biol. **124:**55–70.
19. **Kuo, L., and P. S. Masters.** 2002. Genetic evidence for a structural interaction between the carboxy termini of the membrane and nucleocapsid proteins of mouse hepatitis virus. J. Virol. **76:**4987–4999.
20. **Macneughton, M. R., and H. A. Davies.** 1978. Ribonucleoprotein-like structures from coronavirus particles. J. Gen. Virol. **39:**545–549.
21. **Narayanan, K., C. J. Chen, J. Maeda, and S. Makino.** 2003. Nucleocapsid-independent specific viral RNA packaging via viral envelope protein and viral RNA signal. J. Virol. **77:**2922–2927.
22. **Narayanan, K., A. Maeda, J. Maeda, and S. Makino.** 2000. Characterization of the coronavirus M protein and nucleocapsid interaction in infected cells. J. Virol. **74:**8127–8134.
23. **Narayanan, K., and S. Makino.** 2001. Cooperation of an RNA packaging signal and a viral envelope protein in coronavirus RNA packaging. J. Virol. **75:**9059–9067.
24. **Nguyen, V. P., and B. G. Hogue.** 1997. Protein interactions during coronavirus assembly. J. Virol. **71:**9278–9284.
25. **Niwa, H., K. Yamamura, and J. Miyazaki.** 1991. Efficient selection for high-expression transfectants with a novel eukaryotic vector. Gene **108:**193–199.
26. **Opstelten, D. J., M. J. Raamsman, K. Wolfs, M. C. Horzinek, and P. J. Rottier.** 1995. Envelope glycoprotein interactions in coronavirus assembly. J. Cell Biol. **131:**339–349.
27. **Rottier, P. J., G. W. Welling, S. Welling-Wester, H. G. Niesters, J. A. Lenstra, and B. A. van der Zeijst.** 1986. Predicted membrane topology of the coronavirus protein E1. Biochemistry **25:**1335–1339.
28. **Sola, I., J. L. Moreno, S. Zuniga, S. Alonso, and L. Enjuanes.** 2005. Role of nucleotides immediately flanking the transcription-regulating sequence core in coronavirus subgenomic mRNA synthesis. J. Virol. **79:**2506–2516.
29. **Thompson, J. D., D. G. Higgins, and T. J. Gibson.** 1994. CLUSTAL W: improving the sensitivity of progressive multiple sequence alignment through sequence weighting, position-specific gap penalties and weight matrix choice. Nucleic Acids Res. **22:**4673–4680.
30. **Tooze, J., and S. A. Tooze.** 1985. Infection of AtT20 murine pituitary tumour cells by mouse hepatitis virus strain A59: virus budding is restricted to the Golgi region. Eur. J. Cell Biol. **37:**203–212.
31. **Vennema, H., G. J. Godeke, J. W. Rossen, W. F. Voorhout, M. C. Horzinek, D. J. Opstelten, and P. J. Rottier.** 1996. Nucleocapsid-independent assembly of coronavirus-like particles by coexpression of viral envelope protein genes. EMBO J. **15:**2020–2028.
32. **Verma, S., V. Bednar, A. Blount, and B. G. Hogue.** 2006. Identification of functionally important negatively charged residues in the carboxy end of mouse hepatitis coronavirus A59 nucleocapsid protein. J. Virol. **80:**4344–4355.
33. **Ye, R., C. Montalto-Morrison, and P. S. Masters.** 2004. Genetic analysis of determinants for spike glycoprotein assembly into murine coronavirus virions: distinct roles for charge-rich and cysteine-rich regions of the endodomain. J. Virol. **78:**9904–9917.
34. **Yount, B., M. R. Denison, S. R. Weiss, and R. S. Baric.** 2002. Systematic assembly of a full-length infectious cDNA of mouse hepatitis virus strain A59. J. Virol. **76:**11065–11078.
35. **Zuniga, S., I. Sola, S. Alonso, and L. Enjuanes.** 2004. Sequence motifs involved in the regulation of discontinuous coronavirus subgenomic RNA synthesis. J. Virol. **78:**980–994.